Available online at www.sciencedirect.com
ScienceDirect
Journal of Sound and Vibration 315 (2008) 1–21
JOURNAL OF SOUND AND VIBRATION
www.elsevier.com/locate/jsvi

Active control experiments on a panel structure using a spatially weighted objective method with multiple sensors

Dunant Halim[a,*], Guillaume Barrault[b], Ben S. Cazzolato[a,1]

[a]School of Mechanical Engineering, University of Adelaide, SA 5005, Australia
[b]Departamento de Engenharia Mecânica, Universidade Federal de Santa Catarina, Florianopolis, SC 88040-900, Brasil

Received 5 October 2006; received in revised form 20 September 2007; accepted 15 January 2008
Handling Editor: J. Lam
Available online 4 March 2008

Abstract

The work describes the experimental implementation of a spatial vibration control strategy using multiple structural sensors distributed over the structure. The control strategy incorporates the spatially weighted vibration objective/performance function that needs to be minimised for achieving vibration control at certain spatial regions. Experiments have been undertaken which were focused on a rectangular panel structure with a number of accelerometers attached. An filtered-X least mean squared (FX-LMS)-based adaptive algorithm has been employed to achieve vibration control at spatial regions of interest by utilising a continuous spatial weighting function. The experimental results demonstrate the effectiveness of the spatial control strategy that can be used for controlling vibration at certain regions that are caused by tonal or broadband excitation.

1. Introduction

A significant amount of research work has been performed on the field of active structural vibration control. Active control strategies can be effectively used to minimise vibration of an entire flexible structure, which is generally caused by low-frequency excitations. In addition to simply minimising vibration of an entire structure, there are cases where it is beneficial to minimise vibration only at certain structural regions. For example, vibration at certain structural regions in a cabin/an acoustic enclosure may be critical for the near-field sound/noise radiation, so the vibration needs to be suppressed. In this case, it is necessary for the developed controller to target vibration at those critical regions, and not at the entire structural region. This way, the control effort can be concentrated on reducing the vibration at the critical spatial regions, which is the main interest of this work.

*Corresponding author at: Australian Centre for Field Robotics, ARC Centre of Excellence in Autonomous Systems, School of Aerospace, Mechanical and Mechatronic Engineering, University of Sydney, NSW 2006, Australia. Tel.: +61 2 9036 7181; fax: +61 2 9351 7474.
E-mail addresses: d.halim@acfr.usyd.edu.au (D. Halim), guillaume.barrault@gmail.com (G. Barrault), benjamin.cazzolato@adelaide.edu.au (B.S. Cazzolato).
[1]Tel.: +61 8 8303 5449

0022-460X/$ - see front matter © 2008 Elsevier Ltd. All rights reserved.
doi:10.1016/j.jsv.2008.01.037

To design an active controller for structural vibration minimisation, model-based control methods such as the optimal $\mathscr{H}_2$ or $\mathscr{H}_\infty$ control methods [1,2] can be utilised. For the cases in which only vibration at certain structural regions need to be controlled, spatial $\mathscr{H}_2$ or $\mathscr{H}_\infty$ control methods [3–7] have been developed, which allow the design of an optimal controller that targets vibration control at certain structural regions. However, there are cases when it may not be practical to obtain a dynamic model of structure for the model-based control design. In such cases, control methods that are less reliant on the a priori dynamic models can provide an alternative method. Such control methods include the work that utilises multiple discrete sensors and spatial interpolations for control design [8,9], and also for generating modal/spatial filters [10–12]. However, the control methods still require a priori structural information such as mass/stiffness or structural modal properties. Other work has also utilised shaped continuous piezoelectric films to generate spatial filters for structural vibration control [13] or for structural sound radiation control [14–17]. In general, the use of piezoelectric films for efficient spatial filtering still requires accurate mode shapes and boundary conditions. It is therefore the aim of this work to provide an alternative control method that depends less on the a priori structural information.

The work presented in this paper focuses on the experimental implementation of active structural vibration control using spatially weighted structural signals introduced in Ref. [18]. The control method allows a continuous spatial weighting to be included in the vibration performance objective so that certain structural regions can be targeted more than other regions. Vibration measurements from sensors are spatially filtered to produce error signals whose energy correspond to the spatially weighted vibration energy to be minimised. A control algorithm based on the filtered-X, least mean squared (FX-LMS) adaptation method can then be used to minimise the relevant spatially weighted vibration energy of the structure.

An advantage of the proposed control method is that it utilises vibration measurements directly from structural sensors, which do not require a priori structural information in terms of mass, stiffness or modal properties, in contrast to previous work in Refs. [8–12]. Contrary to the model-based control methods [3–7], a dynamic model of the structure is also not required, except for the determination of the secondary path model for the implementation of FX-LMS adaptive control.

2. Spatial vibration control using the spatially weighted vibration method

In some cases, it may not be practical to use a model-based control strategy, such as for vibration control applications involving complex structures, whose dynamic models may not be readily available. In this case, non-model-based control is likely to provide a better alternative, in which the structural vibration information can be accessed from a number of structural sensors distributed over a structure. This current work concentrates on the experimental attempts to control the spatial vibration profile of a structure, since the ability to spatially control structural vibration can be advantageous such as for controlling the associated sound radiation. To measure the spatial profile of a vibrating structure, spatial interpolations (such as the one used in numerical finite element method [19,20]) have been employed which are also used in this work. The principle of using spatial interpolations have also been utilised in other work such as in Refs. [8,10] although the approaches still require the information about structural properties.

Consider a flexible structure system, whose vibration at (x, y) location over the structure is observed at the nth sample time, expressed by

$$\mathbf{v}_{xy}(x, y, n) = \mathbf{v}^d_{xy}(x, y, n) + \mathbf{v}^u_{xy}(x, y, n) \tag{1}$$

where $\mathbf{v}^d_{xy}$ and $\mathbf{v}^u_{xy}$, respectively, represent the structural vibration levels due to the disturbance source and control source. Note that in general, $\mathbf{v}_{xy}(x, y, n) \in \mathbb{R}^g$ is a vector quantity with g vibration parameters which could represent the transverse, angular/rotational, strain vibrations, or other vibration measures. If one desires to control the spatial vibration of the structure, it would be desirable to monitor the vibration over the entire structure, and not just at a few structural locations. This may be overcome using the spatial interpolation approach [18]: Fig. 1 depicts an arbitrary panel-type structure with N structural discrete sensors distributed over the structure, in which the ith sensor measures vibration v_i at a particular location (x_i, y_i). Since the vibration level at structural boundaries is often minimal, nodes N_o at the boundaries can be included

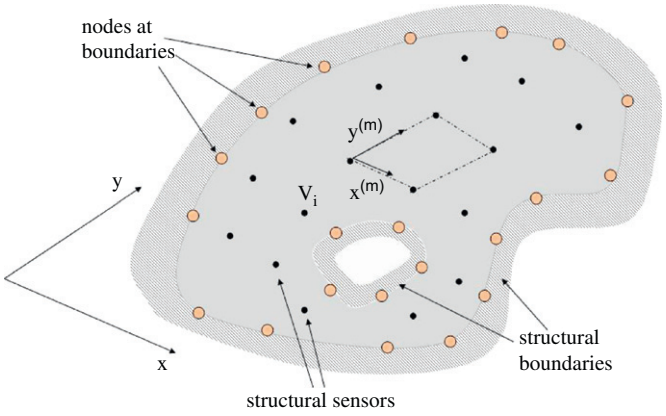

Fig. 1. A panel structure with N structural sensors and N_o nodes at structural boundaries. The vibration level measured by the ith sensor at location (x_i, y_i) is v_i. The mth element has local coordinates of $(x^{(m)}, y^{(m)})$ and is constructed from 4 nodes in this example.

to improve the spatial vibration interpolation, and M elements/regions can then be constructed from $N + N_o$ nodes.

For the mth element/region with local coordinates of $(x^{(m)}, y^{(m)})$, the vibration level $\mathbf{v}_{xy}^{(m)}$ at any location $(x^{(m)}, y^{(m)})$ within the element can be estimated from sensor measurements. If l sensors are used to construct nodes for mth element, $\mathbf{v}_{xy}^{(m)} \in \mathbb{R}^g$ will be the estimated elemental vibration profile which are based from vibration measurements obtained from the sensors, $\mathbf{v}^{(m)}$:

$$\mathbf{v}_{xy}^{(m)}(x^{(m)}, y^{(m)}, n) = \mathbf{H}(x^{(m)}, y^{(m)})\mathbf{v}^{(m)}(n), \tag{2}$$

where $\mathbf{v}^{(m)}$ consists of a group of l vibration measurements associated with the mth element, and $\mathbf{H}(x^{(m)}, y^{(m)})$ is a $g \times l$ interpolation function matrix.

Transforming the local coordinates into the global coordinates using a linear transformation matrix, the vibration at each (x, y) structural location can be estimated from [18]:

$$\mathbf{v}_{xy}(x, y, n) = \mathbf{M}(x, y)\,\mathbf{v}(n), \tag{3}$$

where $\mathbf{v} \in \mathbb{R}^{(N+N_o)}$ consists of vibration measurements v_i and vibrations observed at the nodes. Here, $\mathbf{v}$ consists of vibration signals measured at sensors and at the redundant structural boundary nodes.

2.1. Vibration control at certain spatial regions using spatial weighting

Having obtained the estimated vibration across the structure, structural regions that needs to be controlled can be emphasised using a continuous spatial weighting function, whose values can continuously vary across the structure depending on the control requirement. For instance, transverse vibration at one region may need to be suppressed to reduced sound/noise radiation, while at other region, strain vibration may be suppressed for improvement of structural fatigue performance. A different spatial weighting function can then be employed for each vibration parameter (e.g. transverse or strain vibration) whose high weighting values are given to regions with high-control importance.

In this case, a spatial weighting matrix can be introduced to reflect the spatial regions of interest for vibration control. A real-symmetric spatial weighting matrix $\mathbf{W}(x, y)$ continuous in (x, y) can be introduced where $\mathbf{W}(x, y) > 0$ for all locations $(x, y) \in R$, where R is the structural region of interest. This weighting function can be constructed using polynomial functions in (x, y). The simplest structure for matrix $\mathbf{W}(x, y)$ is a diagonal weighting matrix whose diagonal elements represent the spatial weighting functions for the associated vibration parameters to be controlled.

Thus, one can construct an objective function $J(n)$ representing the spatially weighted vibration energy, which can be minimised using active control strategies [18]. In this case, the instantaneous spatially weighted vibration energy at the nth sample time can be constructed by considering the vibration energy across the

entire surface of a structure:

$$J(n) = \int_R \mathbf{v}_{xy}(x,y,n)^{\mathrm{T}}\,\mathbf{W}(x,y)\mathbf{v}_{xy}(x,y,n)\,\mathrm{d}R = \mathbf{v}(n)^{\mathrm{T}}\left(\int_R \mathbf{M}^{\mathrm{T}}(x,y)\mathbf{W}(x,y)\mathbf{M}(x,y)\,\mathrm{d}R\right)\mathbf{v}(n). \tag{4}$$

Note that a more detailed explanation on the spatially weighted vibration energy of a structure with multiple sensors can be found in Ref. [18]. The above integral term can be calculated by

$$\mathbf{A} = \int_R \mathbf{M}(x,y)^{\mathrm{T}}\mathbf{W}(x,y)\mathbf{M}(x,y)\,\mathrm{d}R = \mathbf{U}\mathbf{V}\mathbf{U}^{\mathrm{T}}, \tag{5}$$

where $\mathbf{V}$ and $\mathbf{U}$ are the eigenvalue and eigenvector matrices obtained from the eigenvalue decomposition of matrix $\mathbf{A}$, respectively. Note that since the term in Eq. (5) is integrated over the entire surface of the structure, the integral term is generally a positive definite matrix. Due to rounding errors that can occur during the numerical integration, the term might consist of a number of small negative eigenvalues. However, the positive definiteness of matrix $\mathbf{A}$ can still be ensured by considering only a number of dominant eigenvalues that will be relevant for control. It will be shown in the experimental results that the satisfactory spatial control performance can be maintained even when only a few dominant eigenvalues are used.

Note that having computed the integral term in Eq. (5), the dimensions of the term can be condensed by removing the appropriate rows and columns that correspond to the associated N_o nodes, which are redundant since vibrations at the nodes (structural boundaries) are minimal [18]. The condensation reduces the dimensions of the term from $N + N_o$ to N. Now, $\tilde{\mathbf{v}} \in \mathbb{R}^N$, which consists of vibration measurements at sensors v_i, can be used for the rest of discussion in this work.

To simplify the control implementation, only a limited number of the largest eigenvalues of $\mathbf{A}$ are actually needed for control. Suppose that $\mathbf{V}$ and $\mathbf{U}$ are reduced in size using the eigenvalue-discarding process such that they now contain only a reduced number of eigenvalues and eigenvectors [18]. The transformed signal $\mathbf{v}_{\mathrm{sp}}(n)$ can now be obtained from the reduced eigenvector and eigenvalue matrices, $\tilde{\mathbf{V}}$ and $\tilde{\mathbf{U}}$:

$$\mathbf{v}_{\mathrm{sp}}(n) = \mathbf{\Omega}_{\mathrm{sp}}\mathbf{v}(n) \approx \tilde{\mathbf{V}}^{1/2}\tilde{\mathbf{U}}^{\mathrm{T}}\tilde{\mathbf{v}}(n). \tag{6}$$

It can be observed that this signal represents the spatially weighted vibration of the entire structure. Thus, an active control strategy that minimises the energy of this signal would lead to the reduction of the spatially weighted structural vibration, i.e. reduction of vibration particularly at certain spatial regions with high weighting values. This instantaneous spatially weighted vibration energy can now be approximated as follows:

$$J(n) = \int_R \mathbf{v}_{xy}(n)^{\mathrm{T}}\mathbf{W}(x,y)\mathbf{v}_{xy}(n)\,\mathrm{d}R \approx \mathbf{v}_{\mathrm{sp}}(n)^{\mathrm{T}}\mathbf{v}_{\mathrm{sp}}(n) = \tilde{\mathbf{v}}(n)^{\mathrm{T}}\mathbf{\Omega}_{\mathrm{sp}}^{\mathrm{T}}\mathbf{\Omega}_{\mathrm{sp}}\tilde{\mathbf{v}}(n), \tag{7}$$

where $\tilde{\mathbf{v}}$ consists of vibration signals measured at sensors.

2.2. Adaptive spatial control using the FX-LMS adaptive control method

Next, the adaptive spatial control implementation using the spatial signal $\mathbf{v}_{\mathrm{sp}}(n)$ can be developed. Let $\mathbf{P}(n)$ and $\mathbf{S}(n)$, respectively, represent the impulse responses at the sensor locations associated with the disturbance $\mathbf{d}(n)$ and control input $\mathbf{u}(n)$. The vibration signal $\mathbf{v}(n)$ can be obtained from

$$\mathbf{v}(n) = \mathbf{P}(n) * \mathbf{d}(n) + \mathbf{S}(n) * \mathbf{u}(n) \tag{8}$$

where $*$ signifies a linear convolution operation.

Consider the case, where the dimension of the spatial signal $\mathbf{v}_{\mathrm{sp}}(n)$ is reduced from potentially N (since N sensors are used) to N_m after the eigenvalue-discarding approach mentioned in Eq. (6), so $\mathbf{v}_{\mathrm{sp}}(n) \in \mathbb{R}^{N_m}$. That is, the first N_m dominant eigenvalues are used for the determination of $\tilde{\mathbf{V}}$ and $\tilde{\mathbf{U}}$. Suppose there are R

disturbance signals $\mathbf{d}(n) \in \mathbb{R}^R$, J reference signals and K control input signals $\mathbf{u}(n) \in \mathbb{R}^K$. The finite impulse response (FIR) adaptive filters using L taps are also utilised for adaptive spatial control.

Thus, the relevant signals can be described as:

$$\mathbf{d}(n) = [d_1(n) \dots d_R(n)]^{\mathrm{T}}$$

$$\mathbf{v}_{\mathrm{sp}}(n) = [v_{\mathrm{sp}\,1}(n) \dots v_{\mathrm{sp}\,N_m}(n)]^{\mathrm{T}}$$

$$\mathbf{x}(n) = [\mathbf{x}_1(n)^{\mathrm{T}} \dots \mathbf{x}_J(n)^{\mathrm{T}}]^{\mathrm{T}}$$

$$\mathbf{x}_j(n) = [x_j(n) \dots x_j(n-L+1)]^{\mathrm{T}}, \quad j = 1, \dots, J$$

$$\mathbf{u}(n) = [u_1(n) \dots u_K(n)]^{\mathrm{T}}$$

$$\mathbf{w}(n) = [\mathbf{w}_1(n)^{\mathrm{T}} \dots \mathbf{w}_K(n)^{\mathrm{T}}]^{\mathrm{T}}$$

$$\mathbf{w}_k(n) = [\mathbf{w}_{k1}(n) \dots \mathbf{w}_{kJ}(n)]^{\mathrm{T}}, \quad k = 1, \dots, K$$

$$\mathbf{w}_{kj}(n) = [w_{kj,0}(n) \dots w_{kj,L-1}(n)]^{\mathrm{T}}, \quad k = 1, \dots, K;\ j = 1, \dots, J, \tag{9}$$

where $\mathbf{x}(n) \in \mathbb{R}^{JL}$ is the reference signal with $\mathbf{x}_j(n) \in \mathbb{R}^L$ containing the last n time-sampled values of the jth reference signal. Also, $\mathbf{w}(n) \in \mathbb{R}^{JKL}$ is the weight vector of K adaptive filters with each filter having the order of L as described in $\mathbf{w}_{kj}(n) \in \mathbb{R}^L$. Interested readers are referred to Ref. [21] for a more detailed discussion on this type of multiple channel adaptive control.

The control input can be calculated from filtering the reference signals with the adaptive weight vector [21]:

$$\mathbf{u}(n) = \mathbf{X}^{\mathrm{T}}(n)\mathbf{w}(n), \tag{10}$$

where $\mathbf{X} \in \mathbb{R}^{JKL \times K}$:

$$\mathbf{X} = \begin{bmatrix} \mathbf{x}(n) & \cdots & \mathbf{0} \\ \vdots & \ddots & \mathbf{0} \\ \mathbf{0} & \mathbf{0} & \mathbf{x}(n) \end{bmatrix}. \tag{11}$$

After the substitution of Eqs. (8) and (10) into Eq. (6), the spatial signal can be obtained:

$$\mathbf{v}_{\mathrm{sp}}(n) = \mathbf{\Omega}_{\mathrm{sp}}(\mathbf{P}(n) * \mathbf{d}(n) - \mathbf{S}(n) * (\mathbf{X}^{\mathrm{T}}(n)\mathbf{w}(n))), \tag{12}$$

where $\mathbf{P}(n)$ contains the $N \times R$ impulse response functions for the primary path; $\mathbf{\Omega}_{\mathrm{sp}}$ is the $N_m \times N$ spatial filter matrix; and $\mathbf{S}(n)$ contains the $N \times K$ impulse response functions for the secondary path that can be estimated using the standard system modelling or identification methods. Thus, each element of $\mathbf{v}_{\mathrm{sp}}$ can be

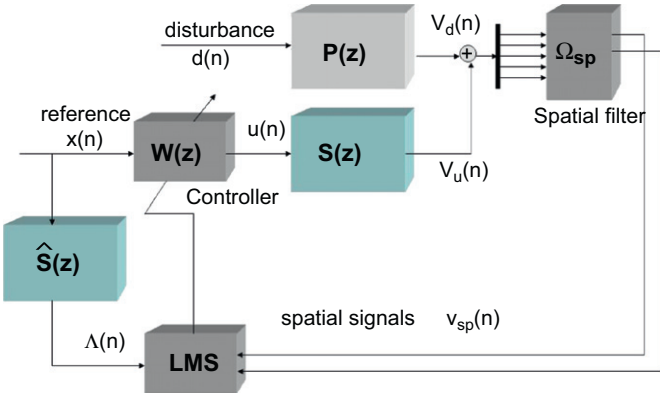

Fig. 2. FX-LMS adaptive spatial control diagram.

shown as

$$v_{\mathrm{sp}\,i}(n) = \mathbf{\Omega}_i \left(\mathbf{P}(n) * \mathbf{d}(n) - \sum_{k=1}^{K} \mathbf{S}_k(n) * \mathbf{w}_k^{\mathrm{T}}(n)\mathbf{x}(n) \right), \quad i = 1, \ldots, N_m, \tag{13}$$

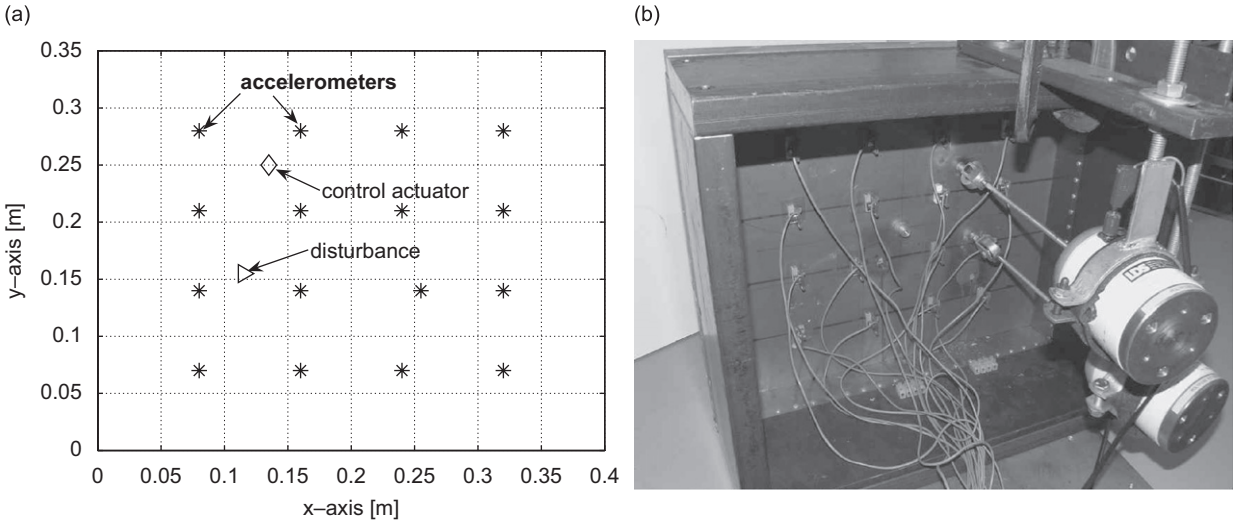

Fig. 3. Experimental set-up for a simply-supported panel structure: (a) locations of 16 accelerometers, disturbance and control actuator; (b) a rectangular panel with the control (top) and disturbance (bottom) actuators.

Table 1
Resonance frequencies of the first five modes of the panel

No.	Mode	Frequency (Hz)
1	(1, 1)	92.5
2	(2, 1)	213.8
3	(1, 2)	261.3
4	(2, 2)	385.0
5	(3, 1)	430.0

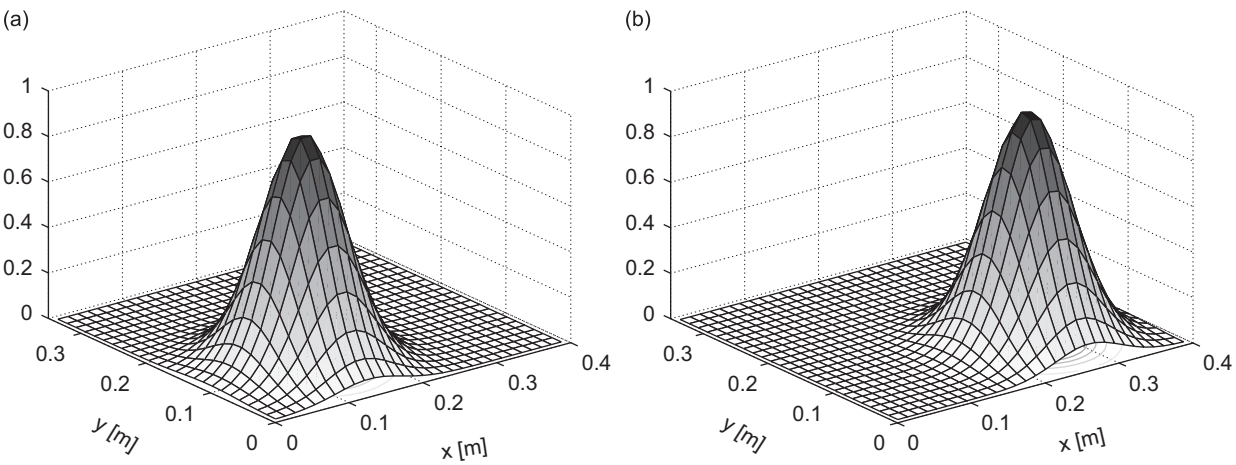

Fig. 4. Two spatial weighting functions used in the experiment: (a) spatial weighting 1, $Q_1(x, y)$; (b) spatial weighting 2, $Q_2(x, y)$.

where

$$\mathbf{S}(n) = [\mathbf{S}_1(n)^{\mathrm{T}} \ldots \mathbf{S}_N(n)^{\mathrm{T}}]^{\mathrm{T}}$$

$$\mathbf{\Omega}_{\mathrm{sp}}(n) = [\mathbf{\Omega}_1(n)^{\mathrm{T}} \ldots \mathbf{\Omega}_{N_m}(n)^{\mathrm{T}}]^{\mathrm{T}}. \tag{14}$$

The adaptive weight vector $\mathbf{w}(n)$ are now adapted using the gradient-based optimisation. Since the minimisation of the spatially weighted vibration is of interest, it can be shown that the optimisation gradient

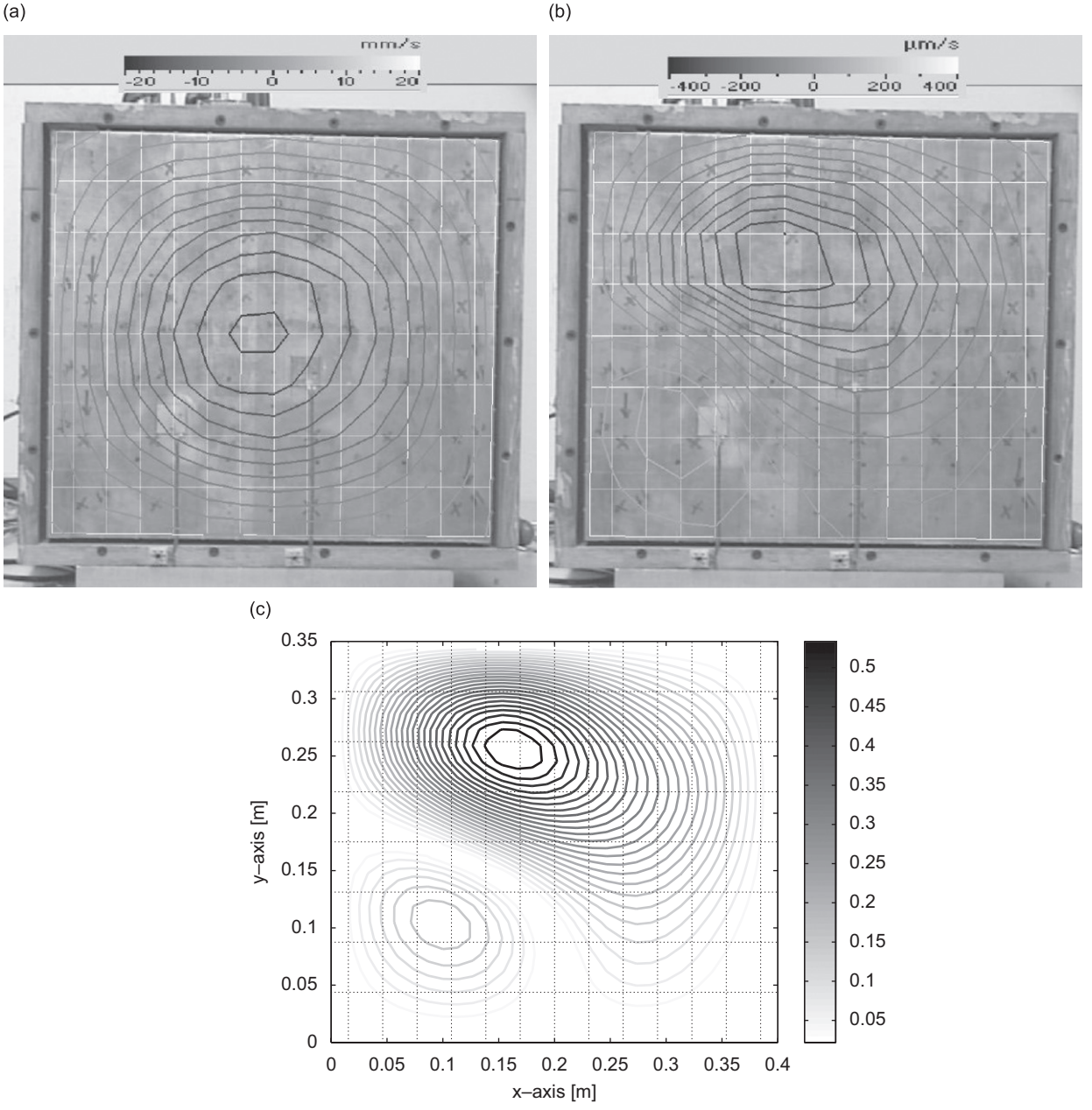

Fig. 5. Experiment using the spatial weighting 1, $Q_1(x, y)$, for mode $(1, 1)$ at 92.5 Hz. The grey-scale bar represents the percentage of vibration level with respect to the maximum uncontrolled vibration: (a) no control—spatial vibration profile of mode $(1, 1)$; (b) with control—experiment; (c) with control—simulation.

has the form of

$$\begin{aligned}\nabla J(n) &= \nabla\left(\int_R \mathbf{v}_{xy}(x,y,n)^{\mathrm{T}}\mathbf{W}(x,y)\mathbf{v}_{xy}(x,y,n)\,\mathrm{d}R\right)\\ &\approx \nabla(\mathbf{v}_{\mathrm{sp}}(n)^{\mathrm{T}}\mathbf{v}_{\mathrm{sp}}(n))\\ &\approx \nabla\sum_{i=1}^{N_m} v_{\mathrm{sp}\,i}(n)^2.\end{aligned} \tag{15}$$

The gradient with respect to the kth weight $\mathbf{w}_k(n)$ can be found by incorporating Eqs. (13) and (15):

$$\boldsymbol{\nabla}_k \sum_{i=1}^{N_m} v_{\mathrm{sp}\,i}(n)^2 = -2\sum_{i=1}^{N_m} \boldsymbol{\Omega}_i \mathbf{S}_k(n) * \mathbf{x}(n) v_{\mathrm{sp}\,i}(n), \tag{16}$$

which then leads to the overall gradient with respect to $\mathbf{w}(n)$:

$$\nabla J \approx \boldsymbol{\nabla}\sum_{i=1}^{N_m} v_{\mathrm{sp}\,i}(n)^2 = -2\{\boldsymbol{\Psi}(n) \circledast \mathbf{x}(n)\}\mathbf{v}_{\mathrm{sp}}(n) \tag{17}$$

with

$$\boldsymbol{\Psi} = \begin{bmatrix} \boldsymbol{\Omega}_1\mathbf{S}_1(n) & \boldsymbol{\Omega}_2\mathbf{S}_1(n) & \cdots & \boldsymbol{\Omega}_{N_m}\mathbf{S}_1(n) \\ \boldsymbol{\Omega}_1\mathbf{S}_2(n) & \boldsymbol{\Omega}_2\mathbf{S}_2(n) & \cdots & \boldsymbol{\Omega}_{N_m}\mathbf{S}_2(n) \\ \vdots & \vdots & \ddots & \vdots \\ \boldsymbol{\Omega}_1\mathbf{S}_K(n) & \boldsymbol{\Omega}_2\mathbf{S}_K(n) & \cdots & \boldsymbol{\Omega}_{N_m}\mathbf{S}_K(n) \end{bmatrix}, \tag{18}$$

where $\boldsymbol{\Omega}_i$ is a time-independent matrix and $\circledast$ denotes the Kronecker product convolution which convolve each element of $\boldsymbol{\Psi}(n)$ with vector $\mathbf{x}(n)$.

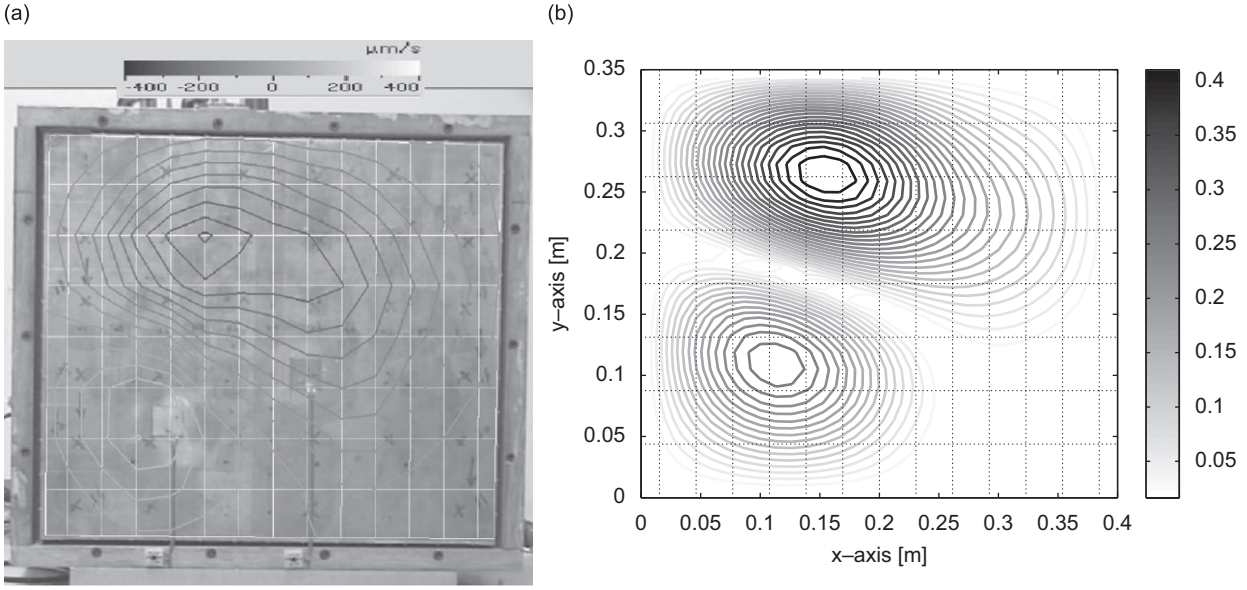

Fig. 6. Experiment using the spatial weighting 2, $Q_2(x,y)$, for mode (1, 1) at 92 Hz. The grey-scale bar represents the percentage of vibration level with respect to the maximum uncontrolled vibration: (a) with control—experiment; (b) with control—simulation.

The adaptation process for the spatial control can now be obtained from:

$$\begin{aligned}\mathbf{w}(n+1) &= \mathbf{w}(n) - \frac{\mu}{2}\nabla J(n)\\ &\approx \mathbf{w}(n) + \mu\mathbf{\Lambda}(n)\mathbf{v}_{\mathrm{sp}}(n),\end{aligned} \tag{19}$$

where μ is the convergence coefficient and $\mathbf{\Lambda}(n)$ is

$$\mathbf{\Lambda}(n) = \mathbf{\Psi}(n) \circledast \mathbf{x}(n). \tag{20}$$

The implementation of the FX-LMS algorithm is illustrated in Fig. 2, where the spatial signal can be obtained from the filtering process of the sensors signals by the spatial filter $\mathbf{\Omega}_{\mathrm{sp}}$. Here, $\mathbf{v}_d$ and $\mathbf{v}_u$ are the vibration signals associated with the disturbance and control inputs, respectively. An adaptive LMS algorithm in Eq. (19) is utilised to optimise the controller coefficients $\mathbf{w}(n)$ that minimises the instantaneous spatially

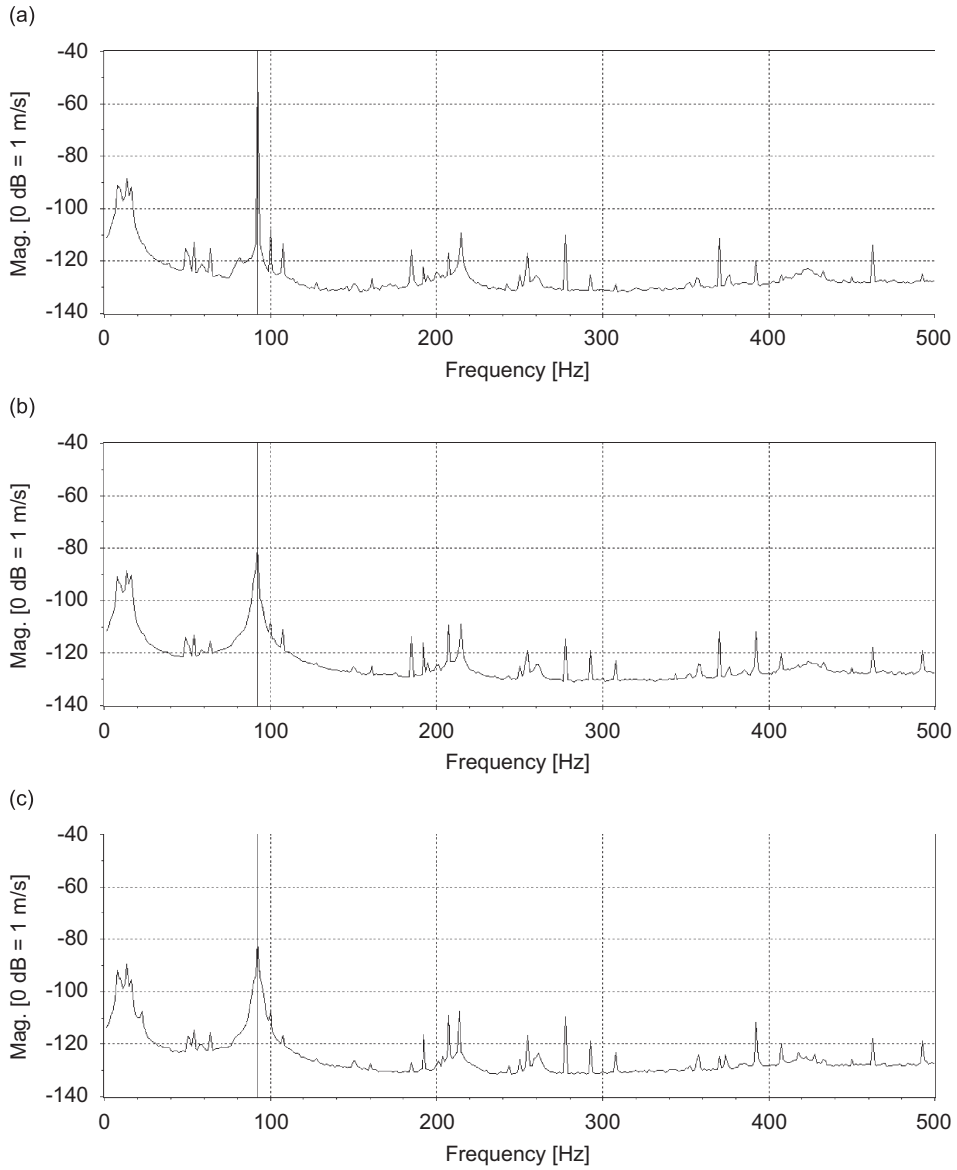

Fig. 7. The average velocity spectrum of the panel for the uncontrolled case, the spatially controlled case with $Q_1(x, y)$, and the spatially controlled case with $Q_2(x, y)$: for mode (1, 1) at 92.5 Hz: (a) no control; (b) spatial control with spatial weighting 1; (c) spatial control with spatial weighting 2.

weighted vibration energy $J(n)$. The following section will describe the implementation of the spatial control strategy to a rectangular panel which is the main part of the work.

3. Experimental implementation of spatial control on a panel structure

For the experiment, a simply-supported steel plate (400 mm × 350 mm × 2.8 mm) was used with $N = 16$ Analog Devices MEMS ADXL50 accelerometers distributed across the plate as shown in Fig. 3. Note that the accelerometers used have the application bandwidth of approximately 500 Hz, which means that only the first 5 structural modes up to a frequency of about 440 Hz can be observed efficiently. Strips of steel sheets are

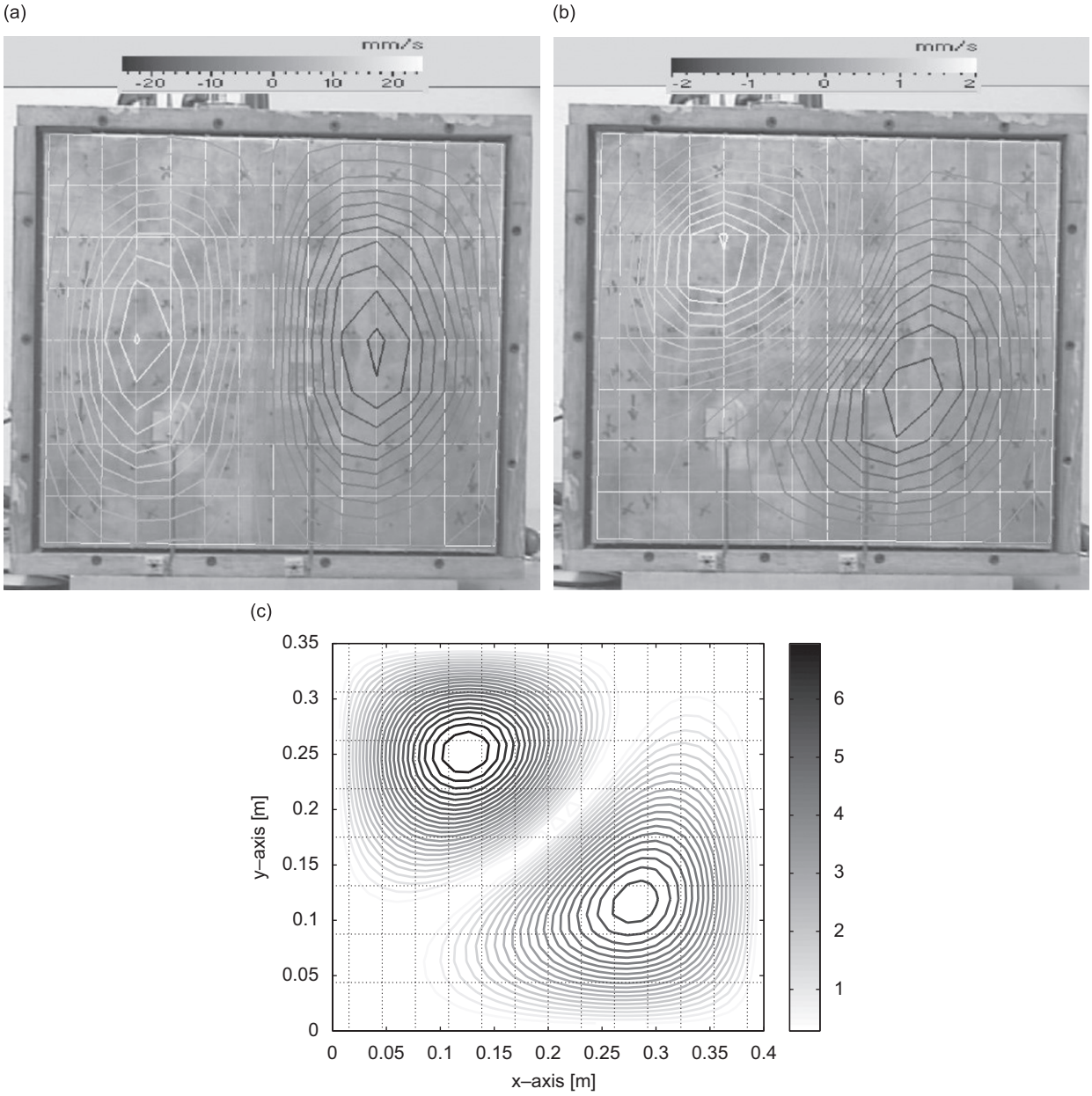

Fig. 8. Experiment using the spatial weighting 1, $Q_1(x, y)$, for mode (2, 1) at 213.8 Hz. The grey-scale bar represents the percentage of vibration level with respect to the maximum uncontrolled vibration: (a) no control—spatial vibration profile of mode (2, 1); (b) with control—experiment; (c) with control—simulation.

attached to the edges of the panel to approximate the simply-supported (or pinned) boundary conditions. Only 5 largest eigenvalues are used to create the spatial filter $\mathbf{\Omega}_{sp}$ which means that the spatial signals produced by the 16 accelerometers have the dimensions of only 5, reducing the need to use a large number of inputs for the error signals used for the adaptive control.

Two LING V-200 electrodynamic shakers were used as disturbance and control sources whose locations are shown in Fig. 3. The placements of shakers were not optimised since the main interest of the work is to demonstrate the effectiveness of the proposed adaptive spatial control. However, the positions of both shakers allowed excitation of the first 5 resonances of the panel. The 5 lowest resonance frequencies are shown in Table 1. An electronic filtering box was used to implement the spatial filtering based on matrix $\mathbf{\Omega}_{sp}$ and EZ-ANC II controller was used to implement the FX-LMS based spatial feedforward control by utilising the spatial signals $\mathbf{v}_{sp}(n)$ with a sampling frequency of 5 KHz.

The vibration signals from the accelerometers were initially filtered to obtain spatial signals that represent the spatially weighted vibration of the entire panel. The energy of the spatial signals can be minimised by employing the FX-LMS adaptation algorithm to generate necessary control actuation via the attached electrodynamic shaker. A Polytec PSV-400-3D laser scanning vibrometer was then used to obtain velocity measurements at 9×15 points across the panel structure.

For the experiment, linear interpolations and rectangular elements/regions were used to obtain the matrix of interpolation functions in Eq. (2). Each rectangular element thus consisted of $l = 4$ sensors at all 4 corners with the elemental dimensions of $h_x^{(m)}$ and $h_y^{(m)}$ (in $x^{(m)}$ and $y^{(m)}$ directions, respectively). The linear interpolation matrix used is

$$\mathbf{H}(x^{(m)}, y^{(m)}) = \begin{bmatrix} \left\{1 - \left(\frac{x^{(m)}}{h_x^{(m)}}\right)\right\}\left\{1 - \left(\frac{y^{(m)}}{h_y^{(m)}}\right)\right\} \\ \left(\frac{x^{(m)}}{h_x^{(m)}}\right)\left\{1 - \left(\frac{y^{(m)}}{h_y^{(m)}}\right)\right\} \\ \left\{1 - \left(\frac{x^{(m)}}{h_x^{(m)}}\right)\right\}\left(\frac{y^{(m)}}{h_y^{(m)}}\right) \\ \left(\frac{x^{(m)}}{h_x^{(m)}}\right)\left(\frac{y^{(m)}}{h_y^{(m)}}\right) \end{bmatrix}^{\mathrm{T}}. \tag{21}$$

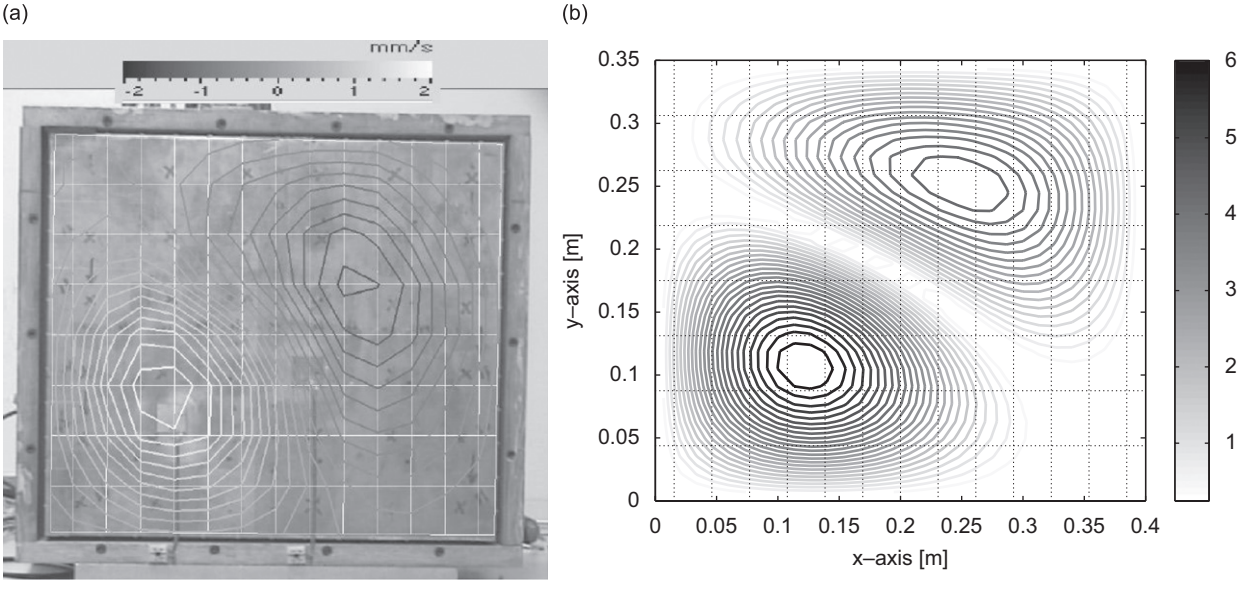

Fig. 9. Experiment using the spatial weighting 2, $Q_2(x, y)$, for mode (2, 1) at 213.8 Hz. The grey-scale bar represents the percentage of vibration level with respect to the maximum uncontrolled vibration: (a) with control—experiment; (b) with control—simulation.

To test the effectiveness of the proposed spatial control, a number of different spatial weightings can be used. In this work, it was decided to concentrate the work on achieving vibration reduction at certain localised spatial regions, instead of the entire region of the structure. Therefore, the experiments utilised two representative spatial weighting functions that emphasised two different spatial regions. The two normalised scalar spatial weightings $Q_1(x,y)>0$ and $Q_2(x,y)>0$ are shown in Fig. 4 and spatial filter matrix $\mathbf{\Omega}_{sp}$ can be obtained from Eq. (6). Note that the two weighting functions have different structural regions of interest as reflected by the high weighting values. In this case, spatial weightings 1 and 2 have maximum weightings at (0.133, 0.110 m) and (0.265, 0.100 m), respectively. Note that the centre of the panel is located at (0.200, 0.175 m) so the peak of spatial weighting 1 occurs closer to the centre of the panel compared to that of spatial weighting 2. The purpose of these spatial weightings is to target regions where vibration control is desirable.

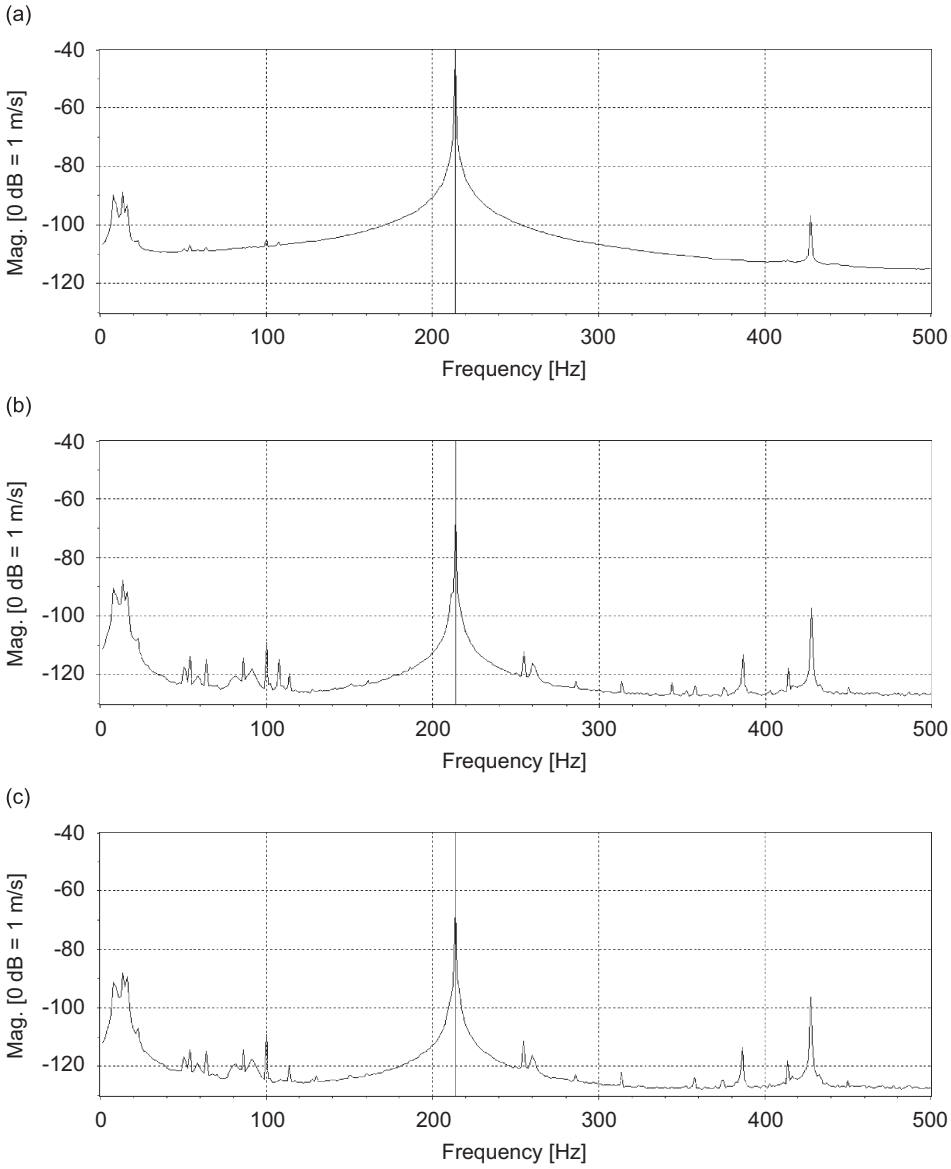

Fig. 10. The average velocity spectrum of the panel for the uncontrolled case, the spatially controlled case with $Q_1(x,y)$, and the spatially controlled case with $Q_2(x,y)$: for mode (2, 1) at 213.8 Hz: (a) no control; (b) spatial control with spatial weighting 1; (c) spatial control with spatial weighting 2.

3.1. Spatial tonal control of a panel structure

In this section, vibration control experiments at a single excitation frequency were performed to observe the effectiveness of spatial tonal control. Since significant vibration occurred at or near the structural resonance frequencies, the experiments targeted a number of resonance frequencies.

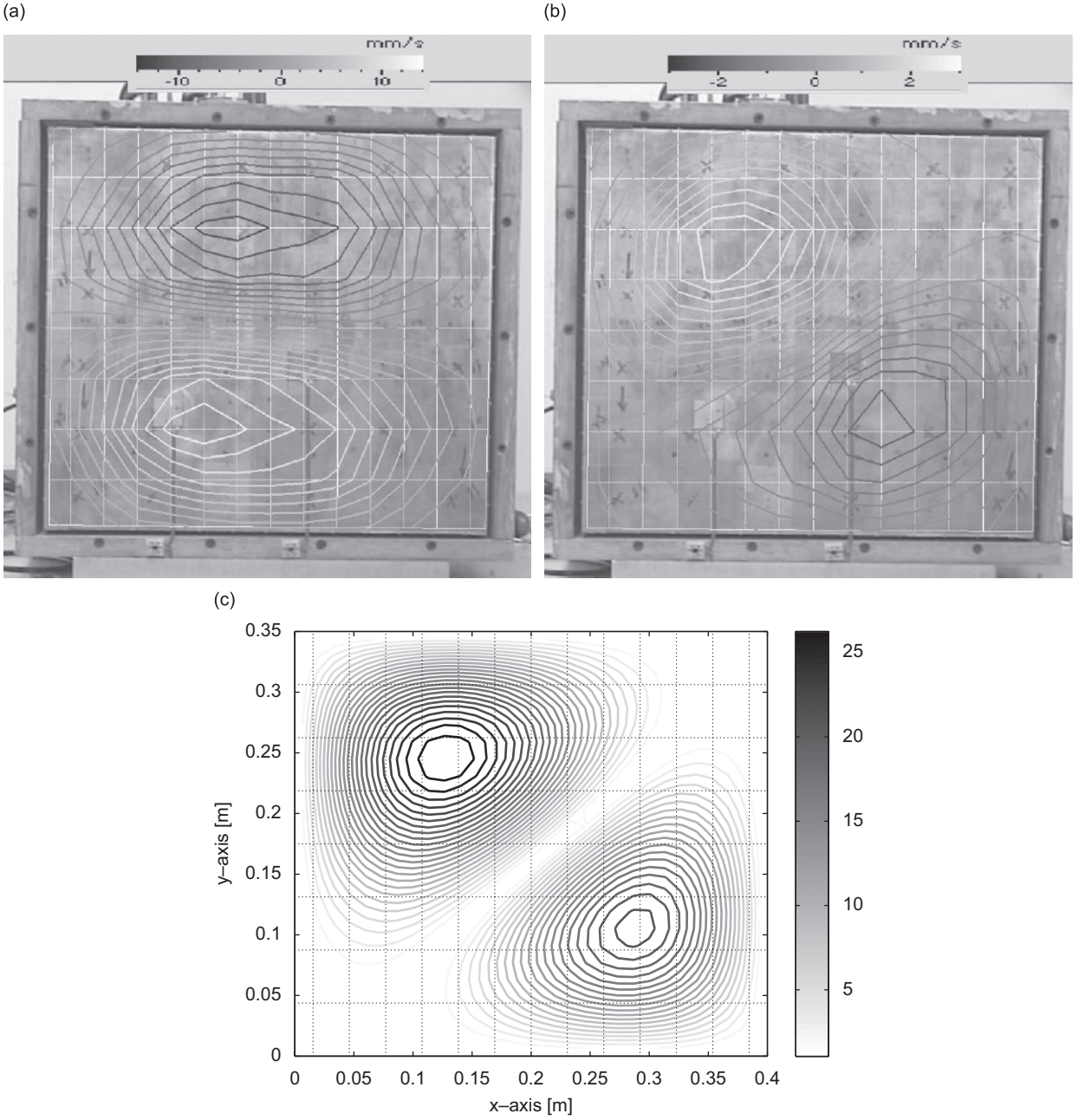

Fig. 11. Experiment using the spatial weighting 1, $Q_1(x, y)$, for mode (1, 2) at 261.3 Hz. The grey-scale bar represents the percentage of vibration level with respect to the maximum uncontrolled vibration: (a) no control—spatial vibration profile of mode (1, 2); (b) with control—experiment; (c) with control—simulation.

3.1.1. *Spatial control on mode* (1, 1) *at 92.5 Hz*

The first experiment considered the first structural mode (1, 1) at 92.5 Hz. The root mean squared (rms) vibration profile of the panel with and without control are shown in Fig. 5 for the control case using the spatial weighting 1. It can be seen that the vibration at the structural region of interest (at the lower left-hand side (LHS) corner of the panel) has been reduced more than the upper region as expected. The vibration nodal line occurred closer to the region of interest, which implies that the upper and lower regions vibrated in opposite directions (i.e. with 180° phase difference). The simulation result based on an idealised simply-supported panel using an optimal spatial tonal control approach is also shown in Fig. 5(c). Interested readers are referred to Ref. [18] for a more detailed explanation about this optimal spatial tonal control approach. It is interesting to note that the spatial vibration profiles obtained from the experiment and the idealised model were reasonably similar. At higher frequencies, however, more pronounced differences between the experiment and simulation could be expected since the simulation model was an ideal simply-supported panel which was based on the modal analysis method with the truncation of higher frequency modes.

When the spatial weighting 2 was used for spatial control, the control results (shown in Fig. 6) are different from those for the spatial weighting 1 case. The region with minimal vibration, represented by the vibration nodal line, had been shifted closer to the lower right-hand side (RHS) corner of the panel, which was the structural region of interest for the spatial weighting 2. As the consequence, the vibration level at the lower LHS corner had been increased compared to that of the previous case. Thus, it can be seen that the implemented spatial control was able to minimise vibration at the spatial region of interest by using only a single control actuator. The control performances could be improved further by increasing the number of control actuators used.

Fig. 7 shows the average velocity spectrum based on 9×15 points scanning laser measurements across the panel. It is interesting to note that below 20 Hz there was a significant vibration observed in the spectrum, which was caused by background vibration in the laboratory. However, the background vibration occurred at very low frequencies, below the first resonant mode of the panel so it would not significantly influence the spatial control experiments. For both control cases that used different spatial weightings, the averaged vibration reductions of the panel were approximately 35 and 36 dB at 92.5 Hz, respectively, for spatial weightings 1 and 2. The results were expected since the overall panel vibration had also been reduced, although the region of interest had received more vibration reduction as shown in Figs. 5 and 6.

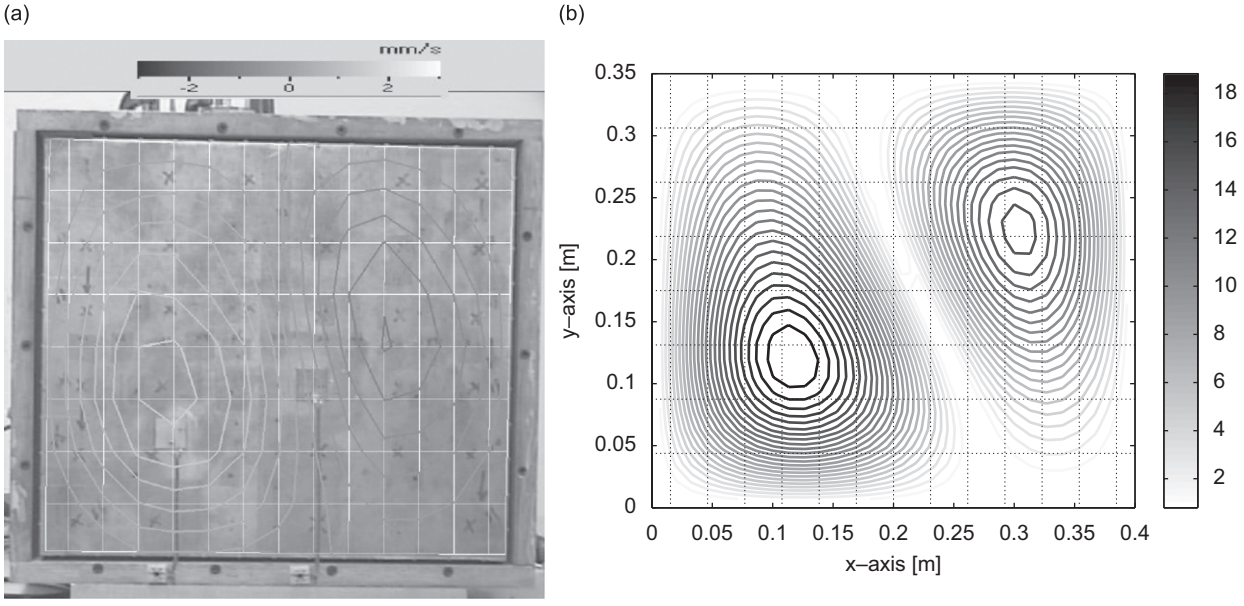

Fig. 12. Experiment using the spatial weighting 2, $Q_2(x, y)$, for mode (1, 2) at 261.3 Hz. The grey-scale bar represents the percentage of vibration level with respect to the maximum uncontrolled vibration: (a) with control—experiment; (b) with control—simulation.

3.1.2. *Spatial control on mode* (2, 1) *at 213.8 Hz*

Experimental results for mode (2, 1) at 213.8 Hz are shown in Figs. 8 and 9 for spatial control using spatial weightings 1 and 2, respectively. After control, it can be observed that the regions of low vibration actually occurred around a diagonal nodal line over the panel. The results were expected since for the spatial weighting 1 case, the diagonal nodal line cut across the lower LHS region, which was the region of interest for vibration minimisation. Similarly for the spatial weighting 2 case shown in Fig. 9, the controller also targeted structural vibration at the lower RHS region. Simulation results also describe similar patterns of results for both control cases. Fig. 10 shows the average velocity spectrum across the panel, where for both control cases, the average vibration reductions of the panel were similar at approximately 22.5 dB at the resonance frequency of mode (2, 1) of 213.8 Hz.

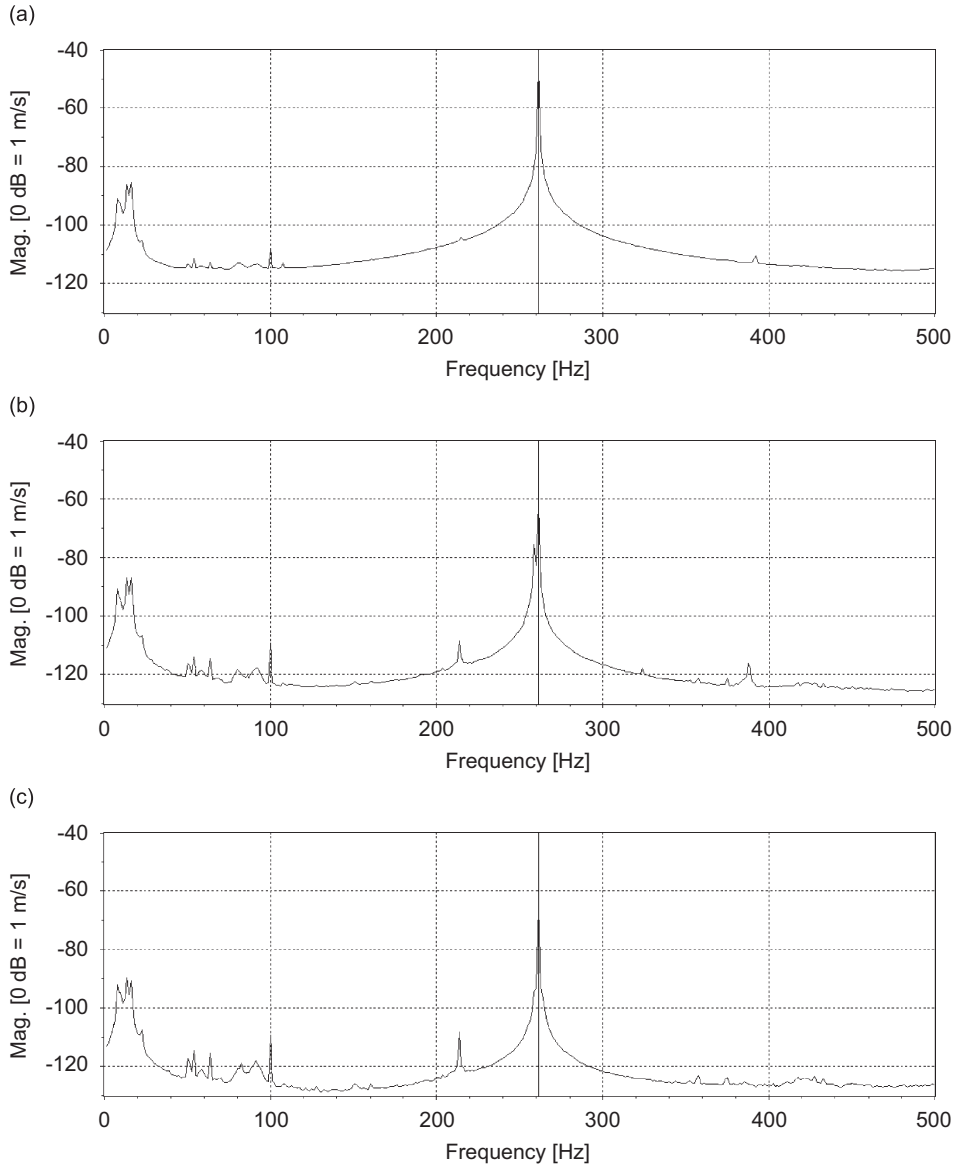

Fig. 13. The average velocity spectrum of the panel for the uncontrolled case, the spatially controlled case with $Q_1(x, y)$, and the spatially controlled case with $Q_2(x, y)$: for mode (1, 2) at 261.3 Hz: (a) no control; (b) spatial control with spatial weighting 1; (c) spatial control with spatial weighting 2.

3.1.3. Spatial control on mode (1, 2) at 261.3 Hz

Control results for mode (1, 2) at 261.3 Hz are shown in Figs. 11 and 12 for spatial control using spatial weightings 1 and 2, respectively. Again a diagonal nodal line indicated the location where the vibration level was lower than that at other regions. The implemented controller had modified the vibration profile of the panel at that particular frequency so that the structure had a minimal spatially weighted vibration energy. Simulation results also indicated a similar control behaviour, indicating the actual control results agreed well with the idealised optimal spatial control results. The average velocity spectrum across the panel is shown in

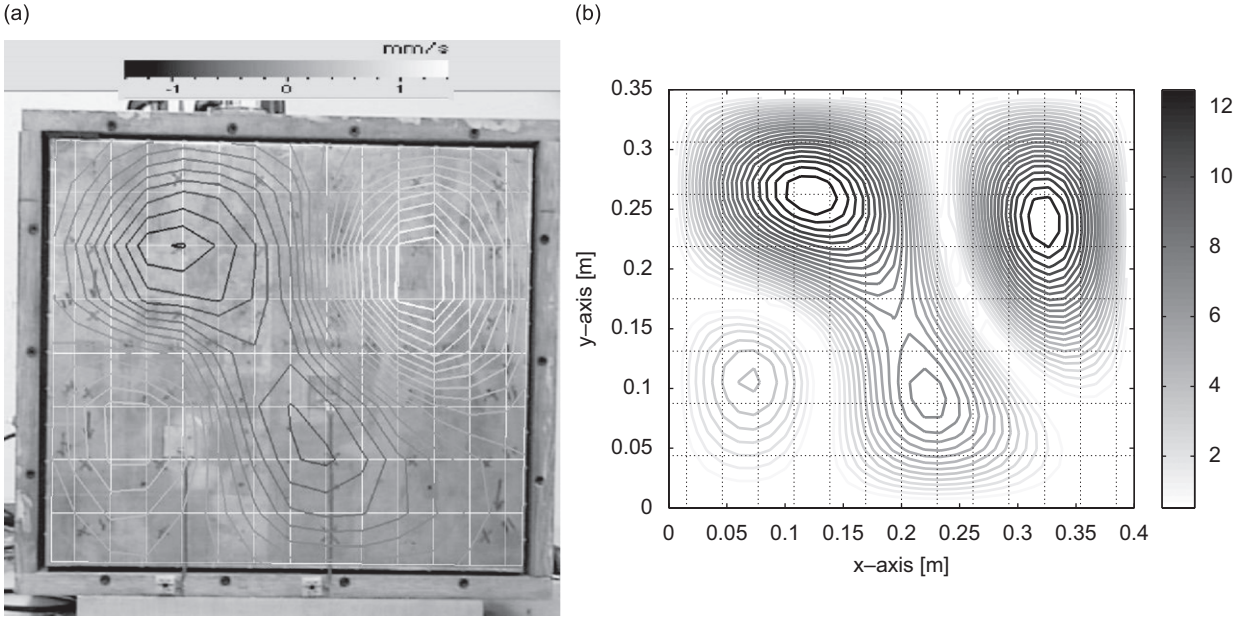

Fig. 14. Experiment using the spatial weighting 1, $Q_1(x, y)$, for mode (2, 2) at 385.0 Hz. The grey-scale bar represents the percentage of vibration level with respect to the maximum uncontrolled vibration: (a) with control—experiment; (b) with control—simulation.

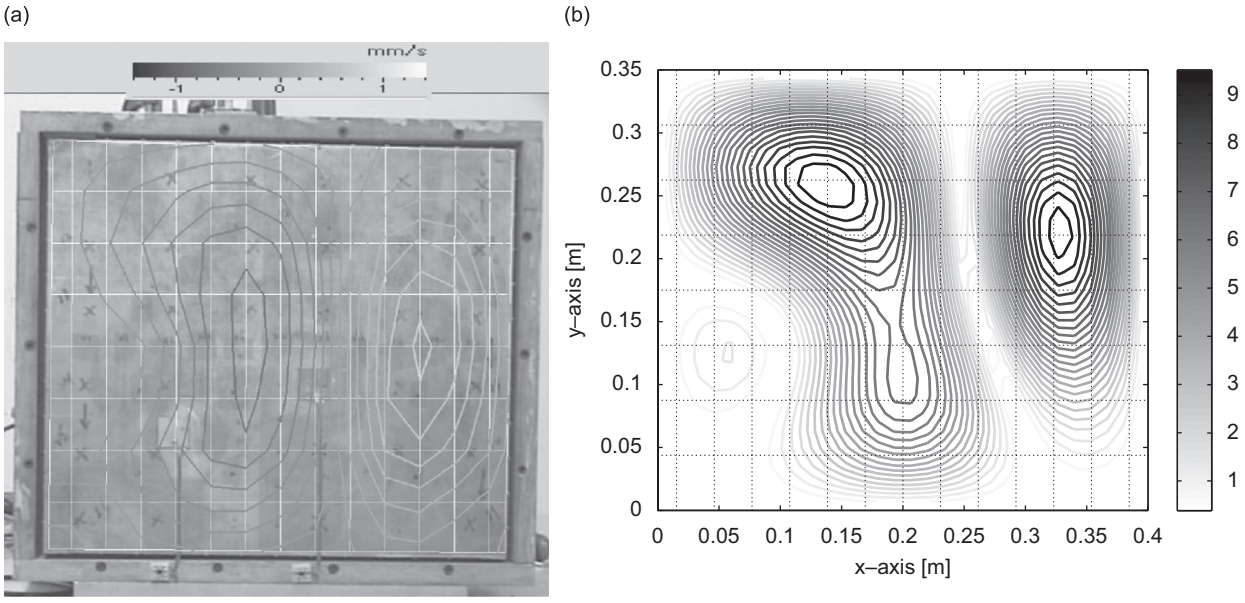

Fig. 15. Experiment using the spatial weighting 2, $Q_2(x, y)$, for mode (2, 2) at 385.0 Hz. The grey-scale bar represents the percentage of vibration level with respect to the maximum uncontrolled vibration: (a) with control—experiment; (b) with control—simulation.

Fig. 13. The average panel vibration reduction levels for the spatial weighting 1 and 2 cases were, respectively, 15.5 and 19.5 dB at the resonance frequency of mode (1, 2) of 261.3 Hz.

3.1.4. *Spatial control on mode* (2, 2) *at 385.0 Hz*

The experimental results for spatial control on the mode (2, 2) at 385.0 Hz are shown in Figs. 14 and 15 for the cases with spatial weightings 1 and 2 respectively. There were two main nodal lines occurring across the surface of the controlled panel. For the spatial weighting 1 case, a nodal line occurred at the lower LHS of the panel, cutting across the region with the maximum spatial weighting at (0.133, 0.110 m). For spatial weighting 2 case, a nearly vertical nodal line (compared to Fig. 14) occurred closer to the RHS of the panel so that the vibration at the lower RHS could be suppressed further. The nodal line also cut across the region around (0.265, 0.100 m) which had the maximum weighting for the spatial weighting 2 case.

It should be noted that the ability of a single control actuator to modify a spatial vibration profile can be limited particularly for vibration modes with high-spatial variations. Thus for higher frequency vibration control, an improved spatial vibration regulation can be achieved by increasing the number of control actuators. In addition, the number of sensors used can also limit the control performances since vibration modes with high-spatial variations will require a more spatially dense sensor arrangement to estimate the structural vibration profile more accurately.

3.2. *Spatial broadband control on a panel structure*

The following experiment focussed on broadband control of the panel since broadband structural vibration could also occur in practice. The experiment had targeted the broadband vibration arising from the first 5 structural modes here since the application bandwidth of the accelerometers was limited to approximately 500 Hz. The scanning laser vibrometer was used to measure the rms vibration level at a number of points across the panel. The vibration profiles for the uncontrolled panel are shown in Fig. 16. The simulation results were obtained by finding an optimal controller that minimised the spatially weighted cost function using an optimal $\mathscr{H}_2$ control strategy.

It can be shown that both simulation and experimental results show a similar rms vibration profile with the highest vibration energy occurring in the middle of the panel. From the results, it can be seen that the contribution of the first 3 modes (1, 1), (2, 1) and (1, 2) at 92.5, 213.8, 261.3 Hz was significant such as shown in

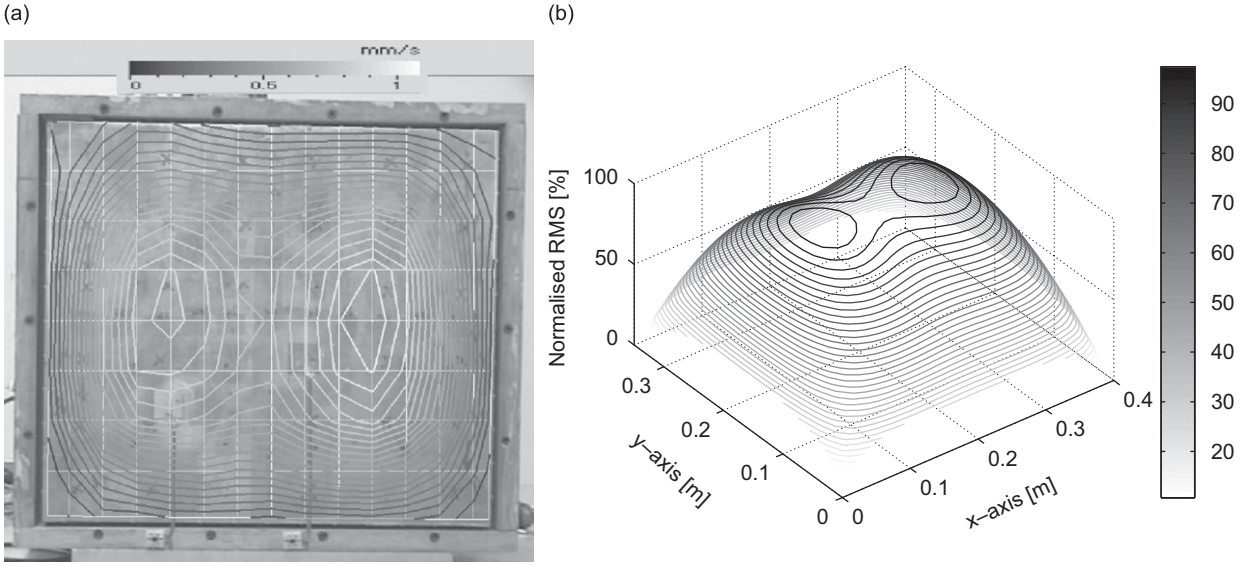

Fig. 16. Rms broadband vibration profile for the uncontrolled panel: (a) experiment; (b) simulation.

the average velocity spectrum depicted in Fig. 17(a). The effect of spatial control on the broadband vibration profile is shown in Fig. 18(a) for the spatial weighting 1. The maximum vibration regions of the controlled panel still occurred at the LHS and RHS regions of the panel, which were similar to those of the uncontrolled panel. However the overall vibration had decreased with the maximum rms vibration (occurring around the centre of the panel) being reduced from 1.1 mm/s (as shown in Fig. 16(a)) to 0.6 mm/s (Fig. 18(a)).

Furthermore, note that due to the control action, the LHS vibration peak had been shifted up relative to the RHS vibration peak. The results were expected since the lower LHS region had a high weighting indicated by the spatial weighting 1, which meant that more vibration reduction was desirable at the lower LHS region. A similar vibration profile was observed from the simulation as depicted in Fig. 18(b) where the RHS vibration peak had been also shifted up by control action (the region of interest was shown with a circle). From Fig. 17(b), the average vibration reductions achieved were 8, 7, 12 and 11 dB for the first 4 modes.

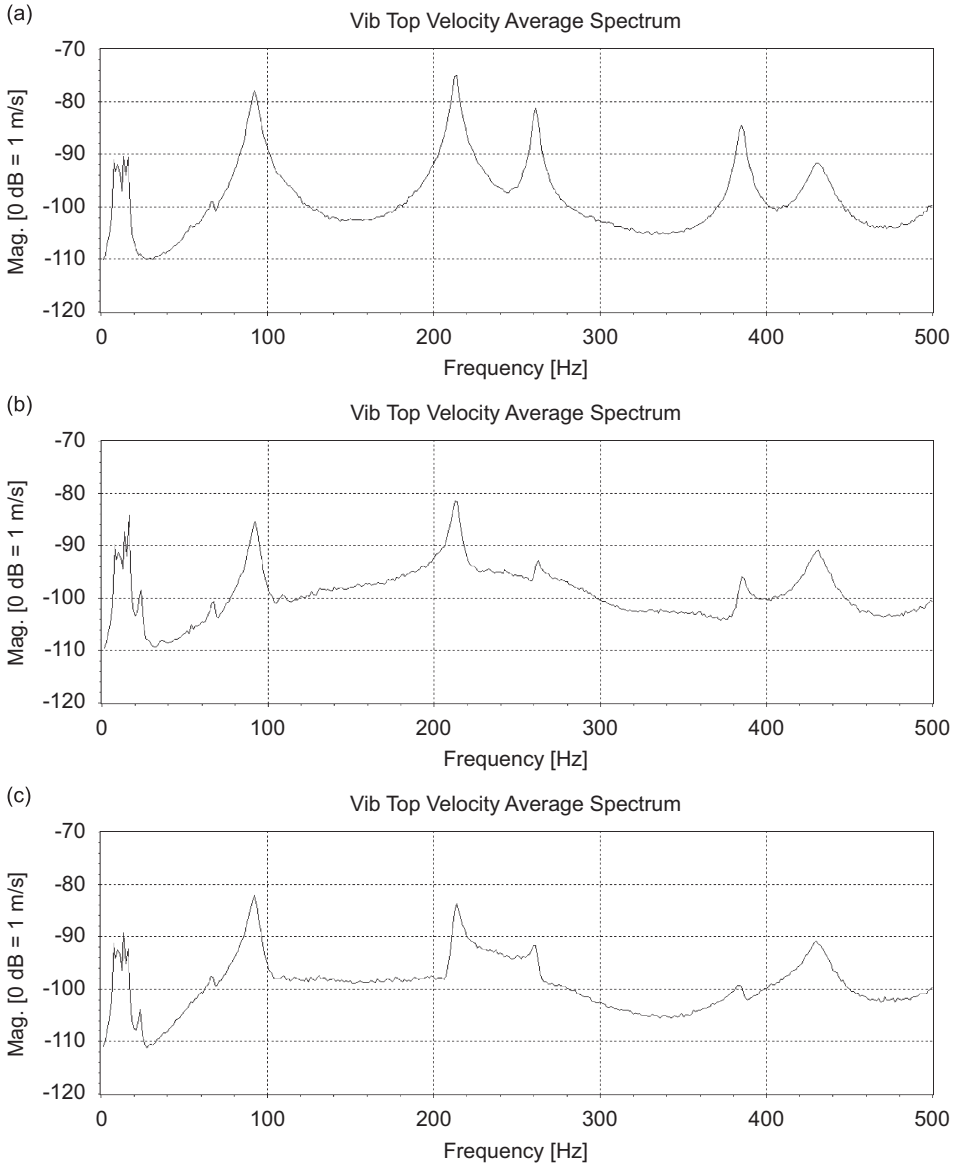

Fig. 17. The average velocity spectrum of the panel for the uncontrolled case, spatially controlled case with $W_1(x,y)$, and spatially controlled case with $W_2(x,y)$: (a) no control; (b) spatial control with spatial weighting 1; (c) spatial control with spatial weighting 2.

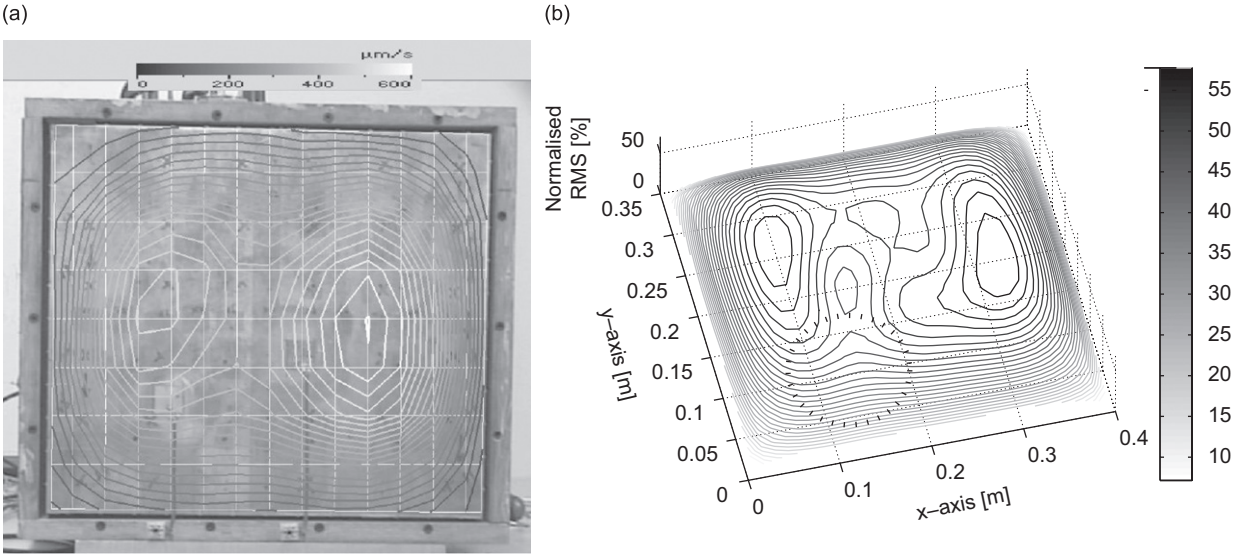

Fig. 18. Rms broadband vibration profile for the controlled panel: experiment and simulation using the spatial weighting 1, $Q_1(x, y)$. Dashed circle shows the spatial region of interest for control: (a) experiment; (b) simulation.

However, there was a 1 dB vibration increase observed for the 5th mode (3, 1) at 430 Hz. Note that since the broadband case involved simultaneous excitations of a number of structural modes, the spatial vibration variation was less pronounced than that for tonal cases. In addition, increasing the number of control sources could also improve the broadband spatial control performance in targeting specific regions.

The broadband spatial control results for the spatial weighting 2 is shown in Fig. 19. In this case, the vibration peak at the RHS region had been shifted up since the spatial region of interest was located at the lower RHS region of the panel. The overall vibration had also decreased with the maximum rms vibration being reduced from 1.1 to 0.6 mm/s. Note that the simulation results in Fig. 19(b) shows a similar vibration profile as observed from the experiments. When the control gain was increased, Fig. 19(c) indicates that the broadband energy was further reduced in the lower RHS region of interest, so that the vibration in the region shown in a circle could be further reduced. From Fig. 17(c), the averaged vibration reductions achieved were 3, 9, 11 and 14 dB for the first 4 modes, while a 1 dB vibration increase was observed for the 5th mode (3, 1) at 430 Hz.

It is interesting to compare the vibration reduction performance of both control cases shown in Figs. 17(b) and (c). Note that the peak of spatial weighting 1 at (0.133, 0.11 m) was closer to the centre of panel at (0.20, 0.175 m), which was also the vibration peak for mode (1, 1). In contrast, the peak of spatial weighting 2 was closer to the lower RHS corner of the panel. Consequently, the controller for the spatial weighting 1 concentrated more in reducing the strength of mode (1, 1) (by 8 dB) compared to that for the spatial weighting 2 (by only 3 dB). In contrast, the controller for the spatial weighting 2 attempted to reduce the strength of mode (2, 2) (by 14 dB) more than that for the spatial weighting 1 (by only 11 dB) since vibration mode (2, 2) also had the maximum transverse vibration very close to the region of interest (at the lower RHS corner of the panel). In general, the spatial control attempts to control vibration modes that have dominant contributions to vibration at the region of interest. By increasing the number of control actuators used, the control performance can be improved since it allows multiple magnitude and phase control actuations for better regulation of the structural vibration.

4. Conclusions

Experiments on a simply-supported panel structure have been performed in this work, demonstrating the feasibility of implementing the proposed spatial control method for spatial vibration control. The spatial

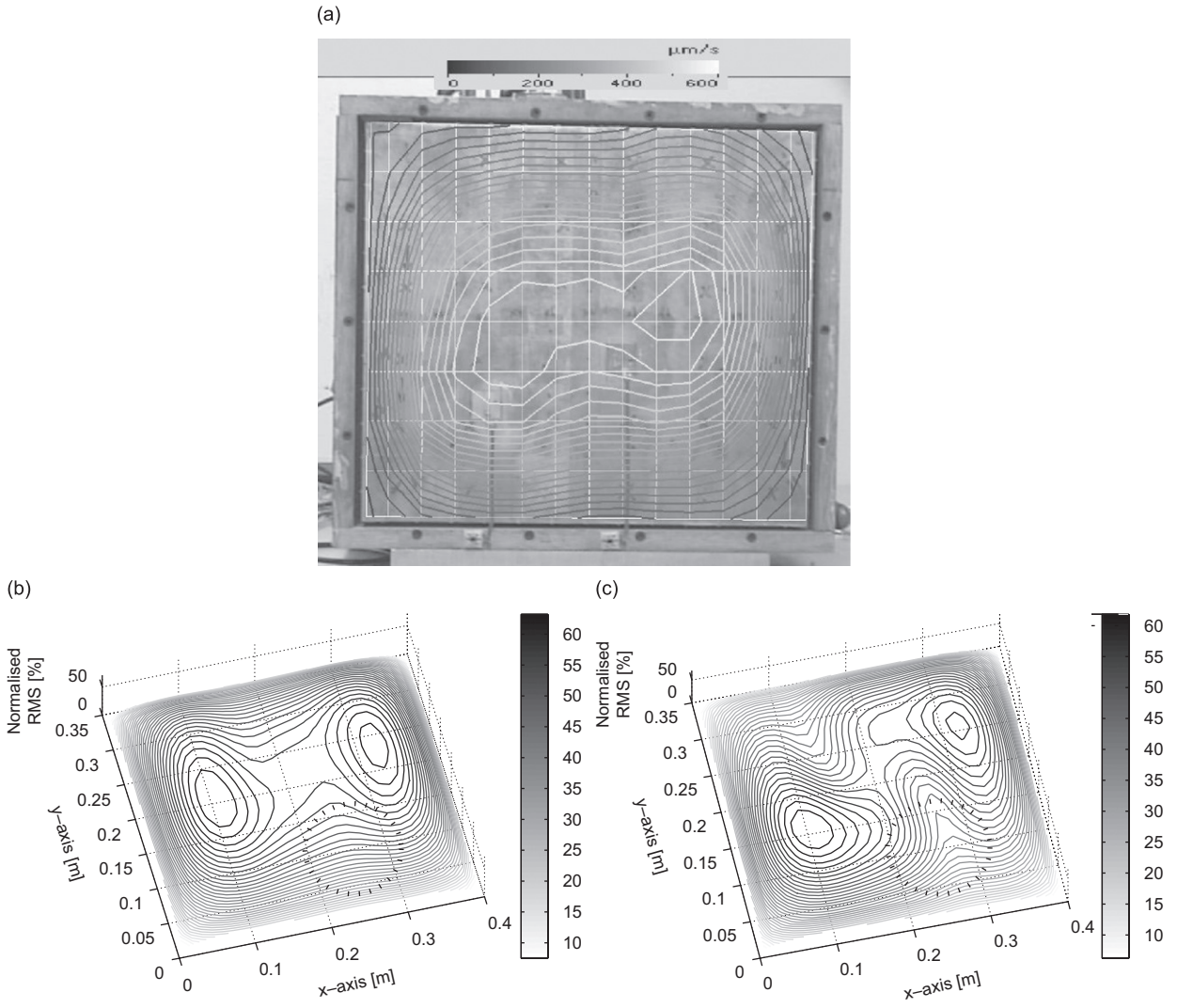

Fig. 19. Rms broadband vibration profile for the controlled panel: experiment and simulation using the spatial weighting 2, $Q_2(x, y)$. Dashed circles show the spatial regions of interest for control: (a) experiment; (b) simulation—control gain 1; (c) simulation—control gain 2.

signal obtained by spatially filtering the sensor signals, represents the spatially weighted vibration over an entire structure that can be utilised for active control. The experiments demonstrated that the spatial control can be utilised to control vibration at particular structural regions. The proposed spatial control can also be used for controlling the associated noise/sound radiated from a vibrating structure. Since the vibration information is obtained directly from structural sensors, apart from the determination of the secondary path model, a dynamic model of the structure is not required in contrast to model-based control, allowing the spatial control method to be used for complex structures whose dynamic models may not be readily available.

Acknowledgements

The authors would like to thank the Australian Research Council (ARC) for its financial support.

References

[1] J.C. Doyle, K. Glover, P.P. Khargonekar, B.A. Francis, State-space solutions to standard $\mathscr{H}_2$ and $\mathscr{H}_\infty$ control problems, *IEEE Transactions on Automatic Control* 34 (8) (1989) 831–847.

[2] K. Zhou, J.C. Doyle, K. Glover, *Robust and Optimal Control*, Prentice-Hall, Englewood Cliffs, NJ, 1996.

[3] S.O.R. Moheimani, M. Fu, Spatial $\mathscr{H}_2$ norm of flexible structures and its application in model order selection, *Proceedings of the 37th IEEE Conference on Decision & Control*, Tampa, Florida, USA, 1998, pp. 3623–3624.

[4] I.R. Petersen, H.R. Pota, Minimax LQG optimal control of a flexible beam, *Proceedings of the 3rd IFAC Symposium on Robust Control Design*, Prague, 2000.

[5] S.O.R. Moheimani, H.R. Pota, I.R. Petersen, Spatial balanced model reduction for flexible structures, *Automatica* 35 (1999) 269–277.

[6] S.O.R. Moheimani, H.R. Pota, I.R. Petersen, Spatial control for active vibration control of piezoelectric laminates, *Proceedings of the 37th IEEE CDC*, Tampa, Florida, 1998, pp. 4308–4313.

[7] S.O.R. Moheimani, D. Halim, A.J. Fleming, *Spatial Control of Vibration: Theory and Experiments*, World Scientific, Singapore, 2003.

[8] G.A. Pajunen, P.S. Neelakanta, M. Gopinathan, M. Arockaisamy, Distributed adaptive control of flexible structures, *SPIE Proceedings of the 1994 North American Conference on Smart Structures and Intelligent Systems* 2190 (1994) 790–801.

[9] M. Gopinathan, G.A. Pajunen, P.S. Neelakanta, M. Arockaisamy, Recursive estimation of displacement and velocity in a cantilever beam using a measured set of distributed strain data, *Journal of Intelligent Material Systems and Structures* 6 (1995) 537–549.

[10] L. Meirovitch, H. Baruh, Control of self-adjoint distributed-parameter systems, *Journal of Guidance* 5 (1) (1982) 60–66.

[11] L. Meirovitch, H. Baruh, The implementation of modal filters for control of structures, *Journal of Guidance* 8 (6) (1985) 707–716.

[12] L. Meirovitch, Some problems associated with the control of distributed structures, *Journal of Optimization Theory and Applications* 54 (1) (1987) 1–21.

[13] S. Collins, D.W. Miller, A. Von Flotow, Distributed sensors as spatial filters in active structural control, *Journal of Sound and Vibration* 173 (4) (1994) 471–501.

[14] R.L. Clark, C.R. Fuller, Modal sensing of efficient acoustic radiators with polyvinylidene fluoride distributed sensors in active structural acoustic control approaches, *Journal of Acoustical Society of America* 91 (6) (1992) 3321–3329.

[15] S.D. Snyder, N. Tanaka, On feedforward active control of sound and vibration using vibration error signals, *Journal of the Acoustical Society of America* 94 (4) (1993) 2181–2192.

[16] F. Charette, A. Berry, C. Guigou, Active control of sound radiation from a plate using a polyvinylidene fluoride volume displacement sensor, *Journal of the Acoustical Society of America* 103 (3) (1998) 1493–1503.

[17] A. Preumont, A. François, P. De Man, N. Loix, K. Henrioulle, Distributed sensors with piezoelectric films in design of spatial filters for structural control, *Journal of Sound and Vibration* 282 (2005) 701–712.

[18] D. Halim, B.S. Cazzolato, A multiple-sensor method for control of structural vibration with spatial objectives, *Journal of Sound and Vibration* 296 (2006) 226–242.

[19] K.J. Bathe, E.L. Wilson, *Numerical Methods in Finite Element Analysis*, Prentice-Hall, Englewood Cliffs, NJ, 1976.

[20] Y.K. Cheung, A.Y.T. Leung, *Finite Element Methods in Dynamics*, Science Press; Kluwer Academic Publishers, Beijing, New York; Dordrecht, Boston, 1991.

[21] S.M. Kuo, D.R. Morgan, *Active Noise Control Systems: Algorithms and DSP Implementations*, Wiley, New York, 1996.